International Journal of Heat and Mass Transfer 104 (2017) 467–477

Contents lists available at ScienceDirect

International Journal of Heat and Mass Transfer

journal homepage: www.elsevier.com/locate/ijhmt

Experimental investigation on a novel multi-branch heat pipe for multi-heat source electronics

Yanghua Cai, Zongtao Li *, Jingmei Zhai, Yong Tang, Binhai Yu

Engineering Research Center of Green Manufacturing for Energy-Saving and New-Energy Technology, South China University of Technology, Guangdong 510640, China

ARTICLE INFO

Article history:
Received 12 May 2016
Received in revised form 24 August 2016
Accepted 24 August 2016
Available online 30 August 2016

Keywords:
Heat pipe
Multi-branch
Thermal management
Multi-heat sources

ABSTRACT

This paper proposes a novel multi-branch heat pipe (MBHP) that can be utilized for heat dissipation in multi-heat source electronics. The proposed heat pipe consists of three branches—two with an evaporator and one with a condenser—connected by vapor lines and liquid lines. A test system was implemented to study the filling ratio, the start-up characteristics, the power distribution characteristics, the dynamic characteristics and the thermal resistance of the heat pipe. The experimental results obtained indicate the following: 1) the optimal working fluid filling ratio of MBHP is between 75% and 100%; 2) the MBHP can start up steadily under tested heating load; 3) the ideal heat load of the MBHP (filling ratio 75%) was within a range of 30–160 W, in which the minimum total thermal resistance was 0.04 °C/W and the maximum temperatures of both evaporators were less than 110 °C under the limiting heating load of 160 W.

1. Introduction

Recently, as a result of steady increases in power and decreases in the volume of electronics, heat dissipation has become an increasingly critical problem that needs to be solved urgently [1]. A heat pipe is a two-phase-exchange heat transfer device with high thermal conductivity that has many advantages including fast heat transfer, good temperature uniformity, stable performance and long lifetime [2–4]. With continuous development of heat pipe technology, heat pipes have become increasingly diverse in terms of structure and shape. Examples of heat pipes include conventional thermosyphon [5], loop heat pipes [6], flat plate heat pipes [7] and pulsating heat pipes [8]. The high efficiency and superior flexibility of heat pipe technology make it an effective approach to solve the heat dissipation problem affecting electronics. It is widely used in areas such as space and aeronautics [9,10], solar energy control [11,12] and waste heat recovery [13].

At present, the vast majority of heat pipes are utilized in heat dissipation of single-heat sources, in which one heat source corresponds to one heat sink. Pastukhov et al. [14] designed the L- and S-shaped micro loop heat pipes predominantly used for heat dissipation of single-heat source high-power microelectronics, such as computer CPU or GPU. Wang [15] studied radiators embedded with multiple U- and L-shaped heat pipes utilized for heat dissipation of a desktop CPU with dimensions 30 mm × 30 mm, minimum thermal resistance values of 0.246 °C/W and 0.166 °C/W, respectively and fairly good conductivity. Lu et al. [16] conducted research on the performance of a high-power LED heat dissipation system that uses a loop heat pipe as the cooling device. It was demonstrated that the junction temperature was controlled below 100 °C under a heat load of 100 W, which guaranteed the performance stability of LED.

With the continuous improvements in miniaturization and integration, electronic devices now contain an increasing number of heat sources. For example, a computer could have multiple CPUs [17,18] and multiple high-power chips could package on the same PCB. For these multi-heat source systems, a heat dissipation scheme comprising multiple heat pipes is conventionally adopted. Ryan et al. [19] employed three heat pipes to implement one-on-one conductive heat dissipation for three chips on the same mainboard of a high-power electronics system, with the aim of guaranteeing that the temperature of chips with a sampling unit power of 230 W is controlled under 70 °C with an ambient temperature of 55 °C. Although this conventional heat dissipation scheme is simple and convenient, it has deficiencies such as large volume, low spatial utilization efficiency difficulty in meeting the requirement of miniaturization for highly integrated devices. Thus, flat plate heat pipes are being seriously considered to solve the problem of multiple heat sources because of advantages such as uniform heat flux and rapid heat transfer [20]. Using mathematical models, Tan et al. [21] analyzed the flow direction and pressure drop of the

* Corresponding author.
E-mail address: meztli@scut.edu.cn (Z. Li).

http://dx.doi.org/10.1016/j.ijheatmasstransfer.2016.08.080
0017-9310/

Nomenclature

A	the wrapped area of the adiabatic cotton (m^2)
A_w	cross-sectional area of the wick (m^2)
D_w	inside diameter of the wick (m)
D	outer diameter of the copper tube (m)
g	gravitational acceleration (m/s^2)
h	gravity distance (m)
K	wick permeability (m^2)
k	thermal conductivity of the adiabatic cotton (W/(m K))
L	latent heat of vaporization (kJ/kg)
l_{eff}	effective length of the heat pipe (m)
l_s	length of the adiabatic section (m)
l_e	length of the evaporator (m)
l_c	length of the condenser (m)
n	totality of the time intervals
Q	total input power (W)
q	heat flux (W/m^2)
r	the capillary radius (m)
V_{powder}	volume of sintered copper powder (m^3)
V	volume of deionized water (m^3)
η	filling ratio
ε	the porosity of the wick
σ	surface tension (kg/s^2)
α	the contact angle
μ_l	dynamic viscosity of liquid (Ns/m^2)
$\dot{m}$	mass flow (kg)
ρ_l	density of liquid (kg/m^3)
Δp	capillary pressure of copper wick (N/m^2)
Δp_{tot}	total pressure drop (N/m^2)
Δp_l	liquid pressure drop (N/m^2)
Δp_v	vapor pressure drop (N/m^2)
Δp_{fl}	pressure drop due to friction (N/m^2)
Δp_g	pressure drop associated to gravity force (N/m^2)
ΔH	thickness of the adiabatic cotton (m)
ΔT_i	the temperature difference across the adiabatic cotton layer (°C)
ΔT	total temperature difference of heat pipe (°C)
$\Delta\tau$	time interval (s)
dT	temperature measurement error of K-type thermocouple (°C)
dW_{power}	output power error of the input power (W)
dT_{data}	resolution of the data acquisition card (°C)
dQ_{ac}	heat leakage of Wrapped adiabatic cotton (W)
T_{ave}	time-averaged temperature of each temperature measurement point (°C)
T_1	temperature of evaporator1 (°C)
T_2	temperature of evaporator2 (°C)
T_3	temperature of evaporator1 branch before merging into condenser branch (°C)
T_4	temperature of evaporator2 branch before merging into condenser branch (°C)
T_5	temperature of evaporator branches after merging into condenser branch (°C)
T_6	temperature of condenser section inlet (°C)
T_7	temperature of condenser branch end (°C)
T_8	ambient temperature (°C)
S	state
R_1	thermal resistance from heat source 1 to concourse of two branches (°C/W)
R_2	thermal resistance from heat source 2 to concourse of two branches (°C/W)
R_3	thermal resistance from concourse of two branches to condenser (°C/W)
R_{tot}	total thermal resistance of heat pipe (°C/W)
U_T	temperature measurement uncertainty
$W(L)$	power of heat source 1 (W)
$W(R)$	power of heat source 2 (W)

Subscripts

ac	adiabatic cotton
ave	average
c	condenser
e	evaporator
max	maximum
tot	total

working liquid in flat plate heat pipes under multiple heat sources. They found that the positional distribution of multiple heat sources on the plane of a flat plate heat pipe was optimized and thus optimal heat transfer performance was obtained. To solve the problem of multiple heat sources, the prerequisite of flat plate heat pipe is that all heat sources should be located on the same plane, making the method inappropriate for heat sources that are spatially scattered or have a staggered distribution. However, for complex positional distribution of heat sources, loop heat pipes may have adequate flexibility to handle the heat source positions problem. Bienert et al. [22] proposed and manufactured a type of loop heat pipe with multiple evaporators. It can start up successfully and solved the problem with different spatial locations and different power values of multiple heat sources. David et al. [23] proposed a multi-evaporator hybrid loop heat pipe and focused on the heat transfer performance of a four-evaporator loop heat pipe that can start normally and operate steadily under a heat load in the range 8–280 W, which is mainly used in spacecraft thermal management. Okutani et al. [24] made the research focuses on multiple-evaporator and multiple-condenser loop heat pipe (MLHP) with polytetrafluoroethylene porous media as wicks. They tested with heat loads to both evaporators to confirm the behavior of the MLHP and tested with heat load to one evaporator to confirm the heat transfer between the evaporators. And when the heat loads were applied to both evaporators, the heat pipe was stably operated up to 40 W/40 W. When the heat load was only applied to one evaporator, the heat pipe was stably operated up to 0 W/50 W. Habtour et al. [25] put forward the miniature multiple evaporator multiple condenser loop heat pipe. The dual-evaporator and dual-condenser was able to successfully transport the heating load from 5 W to 100 W. And the heat pipe demonstrated reliable, robust behavior with one or both evaporators powered, with nonuniform evaporator load, and as power was rapidly switched from one evaporator to another. Although suitable for multi-heat source heat dissipation, loop heat pipes also possess disadvantages such as complex structure, manufacturing difficulty and high cost. In conclusion, there is still no practical effective solution for heat dissipation of multiple heat sources.

Zhou et al. [26] manufactured an anti-gravity loop heat pipe which the outer diameter of copper tube is 8 mm and the overall size is 400 mm * 96.5 mm. The limiting heating load of this heat pipe is about 100 W, when the maximum temperature is lower than 105 °C and the minimum thermal resistance is 0.15 °C. Copper–water wicked heat pipe with a sintered-grooved composite wick, which the outer diameter of copper tube is 8 mm, is developed by Li et al. [27]. Their main study was the effects of vacuuming process parameters on the thermal performance. And the maximum heat transport capacity of the heat pipes could be main-

tained at 100 W with the peak temperature below 100 °C, when the amount of the working fluid was 120% and effective working length is 200 mm. They also fabricated heat pipe samples with other three types of wicks [28], grooved, sintered and grooved with half sintered length. Dimension of all the heat pipe is the outer diameter of 8 mm with the effective working length of 200 mm. All of they can reach the maximum heating load of 100 W except the maximum heating load of sintered wick is only 60 W. Li et al. [29] design the anti-gravity loop-shaped heat pipe and its outer diameter of copper tube is 8 mm. And they found that limiting heat load of the continuous step-graded structure is 70 W while single-powder structure is only 50 W with both the peak temperatures under 110 °C.

Targeting the issue described above, this paper proposes a novel MBHP that collects heat from multiple heat sources and uniformly dissipates with a heat sink. The space occupied by heat pipes can be reduced by using MBHP, which helps to improve the integration level of electronics and miniaturization of electronic devices. To date, to the best of our knowledge, no researcher has ever explored or studied MBHPs. This paper describes the structural design and manufacturing processes of the MBHP, with a focus on its filling ratios, start-up characteristics, power distribution characteristics, dynamic characteristics and thermal resistance.

2. Experiments

2.1. Design, manufacture and theory analysis

Fig. 1 shows (a) the schematic and (b) actual photo of the proposed MBHP. It comprises three sections: two evaporators, a condenser, adiabatic section. The two evaporators are connected in parallel before being connected to the condenser in series. Critical manufacturing parameters of the MBHP are shown in Table 1. The length of each branch of the MBHP is 100 mm, the outer diameter of the copper pipes is 8 mm and the diameter of the vapor lines is 5.5 mm. The inner wall is attached with sintered copper powder with a thickness of 0.85 mm and particle size in the range 75–100 μm. The sintered copper powder provides capillary action to maintain the overall operation of the heat pipe.

Fig. 2 illustrates the manufacturing process of the MBHP. First, three sections of copper pipe are assembled and welded together according to the design using a T-shaped copper joint. A graphite shaft sleeve with stepped concentric holes is then assembled at the end of the longer branch and graphite core rods with a diameter of 5.5 mm are installed to form a T shape at the center of each branch. Next, copper powder is used to fill in the gap between the longer branch and its core rod. Subsequent to the filling, another graphite shaft sleeve is installed at the inlet of the longer branch to prevent leakage of the filled copper powder. Then, a second copper powder filling operation is conducted in the middle branch. Graphite material is used for both core rods and shaft sleeves due to the fact that graphite and copper do not become fused in the process of high-temperature sintering and therefore they can be separated smoothly after sintering. The core rods are then shaped by sintering in an atmospheric furnace at a temperature of 900 °C for 60 min. This method of filling twice and sintering once guarantees that the wicks of the three branches connect with each other to form the whole structure after sintering. Next, the core rods are extracted to form vapor lines. The middle branch is welded and vacuumed, whereas the other two branches are welded and sealed. The branches are then reduced by hydrogen in the atmospheric furnace at 400 °C. Finally, the heat pipe is evacuated to a vacuity of 10^{-3} Pa and injected with Deionized water before being mechanically sealed. Volume of deionized water V can be calculated by the following equation:

$$V = \eta \times \varepsilon \times V_{powder} \tag{1}$$

where η is the filling ratio, ε represent the porosity of the wick, V_{powder} is the volume of sintered copper powder. A MBHP created by following this procedure is shown in Fig. 1(b).

According to Laplace and Young equation, the capillary pressure of copper wick can be formulated by the following.

$$\Delta p = 2\sigma\left(\frac{\cos\alpha_e}{r_e} - \frac{\cos\alpha_c}{r_c}\right) \tag{2}$$

where σ, α and r are the surface tension, the contact angle and the capillary radius. Subscript e and c represent the evaporator and the condenser.

When the heat pipe starts up, the maximum capillary pressure must be greater than the total pressure drop.

$$\Delta p_{\max} \geqslant \Delta p_{tot} = \Delta p_l + \Delta p_v \tag{3}$$

where Δp_{tot}, Δp_l and Δp_v refer to the total pressure drop, the liquid pressure drop and the vapor pressure drop, respectively. The

Table 1
Major features and parameters of the MBHP.

Name	Value/material
Overall size	210 mm × 100 mm
Single evaporator length	30 mm
Condenser length	65 mm
Wall material	Copper
Pipe outer diameter	8 mm
Pipe wall thickness	0.4 mm
Sintered wick material	Copper powder
Sintered wick thickness	0.85 mm
Copper powder particle size	75–100 μm
Working fluid	Deionized water
Porosity	54.5%

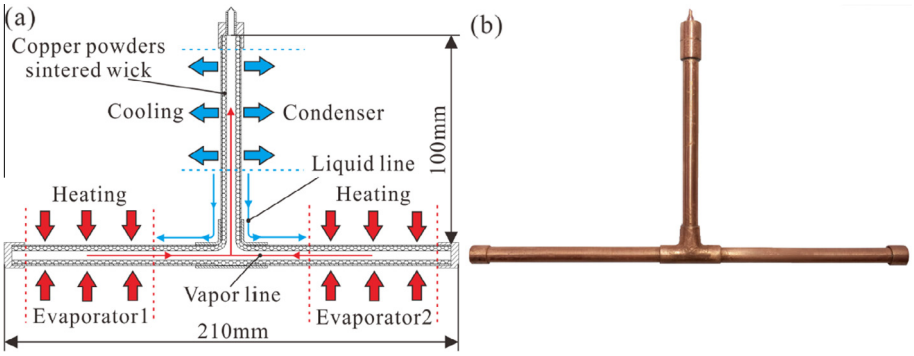

Fig. 1. (a) Mechanism schematic and (b) photo of real device.

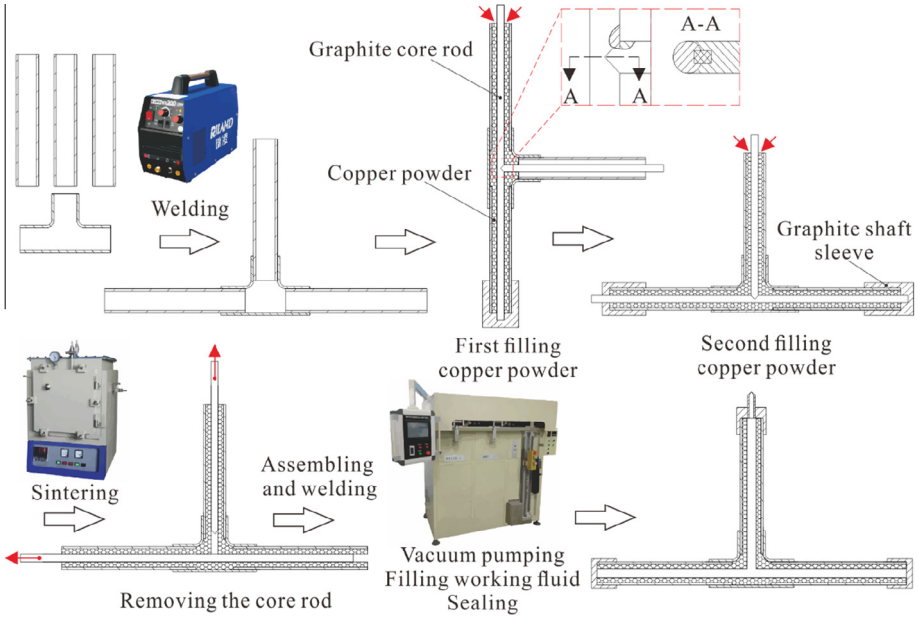

Fig. 2. The MBHP manufacturing process.

maximum capillary pressure and the liquid pressure drop can be calculated from the following formula.

$$\Delta p_{\max} = \frac{2\sigma}{r_e} \tag{4}$$

$$\Delta p_l = \Delta p_{fl} + \Delta p_g \tag{5}$$

where Δp_{fl} and Δp_g are pressure drop due to friction and the pressure drop associated to gravity force. Δp_{fl} may be found by Darcy equation.

$$\Delta p_{fl} = \frac{\mu_l \dot{m} l_{eff}}{\rho_l K A_w} \tag{6}$$

where μ_l, $\dot{m}$, l_{eff}, ρ_l, K and A_w refer to dynamic viscosity of liquid, mass flow, effective length of the heat pipe, density of liquid, wick permeability and cross-sectional area of the wick, respectively. l_{eff} and K can be expressed as below.

$$l_{eff} = l_s + \frac{l_e + l_c}{2} \tag{7}$$

$$K = \frac{D_w^2 \varepsilon^2}{150(1-\varepsilon)^2} \tag{8}$$

where l_s, l_e and l_c are length of the adiabatic section, the evaporator and the condenser. D_w refer to the inside diameter of the wick.

The pressure drop associated to gravity force is as below.

$$\Delta p_g = \rho_l g h \tag{9}$$

where g and h are the gravitational acceleration and the gravity distance.

Ignoring the vapor pressure drop, the maximum mass flow can be got as fellow.

$$\dot{m} = \frac{\sigma \rho_l K A_w}{\mu_l l_{eff}} \left(\frac{2}{r_e} - \frac{\rho_l g h}{\sigma} \right) \tag{10}$$

Therefore, the maximum heat transfer rate of heat pipe can be described by

$$Q = \dot{m} L = \frac{\sigma \rho_l K A_w L}{\mu_l l_{eff}} \left(\frac{2}{r_e} - \frac{\rho_l g h}{\sigma} \right) \tag{11}$$

where L is the latent heat of vaporization.

2.2. Test apparatus

Fig. 3 depicts the heat pipe test apparatus and arrangement. The test system consisted of three modules: heating module, condensing module and temperature data acquisition module. The heating module included two power supplies whose heating power could be adjusted through variable transformers. The condensing module contained aluminum fins and a fan. Forced convection cooling was conducted on the aluminum fins via the fan. The adiabatic section and evaporators were wrapped in a layer of adiabatic cotton to reduce the effect of natural convection when testing. The temperature data acquisition module consisted of eight thermal couples labeled T1–T8, a data acquisition card and a data display and recording system. The installation positions of heat sources and heat sink, as well as the temperature data acquisition positions are shown in Fig. 3. T1 and T4 were used to detect the temperatures of the two evaporators. T2 and T3 were used to detect the temperatures of the evaporator branches before merging into the condenser branch. T5 was used to detect the temperature of the evaporator branches after merging into the condenser branch. T6 was used to detect the temperature of the condenser section inlet. T7 was applied to detect the temperature of the condenser branch end and T8 to detect the ambient temperature.

2.3. Uncertainty analysis

Experimental uncertainty is mainly the random error of the temperature measurement process. Such as K-type thermocouple measurement accuracy of ±0.1 °C, data acquisition card with the resolution of 0.1 °C, the input power tolerance of ±0.5 W.

Temperature measurement uncertainty includes the following independent parts:

(1) temperature measurement error of K-type thermocouple, dT. (2) output power error of the input power, dW_{power}. (3) The resolution of the data acquisition card, dT_{data}. (4) heat leakage of Wrapped adiabatic cotton, dQ_{ac}. The heat leakage of adiabatic cotton can be calculated as follows:

$$dQ_{ac} \approx \sum_1^n \frac{kA\Delta\tau}{\Delta H} \Delta T_i \tag{12}$$

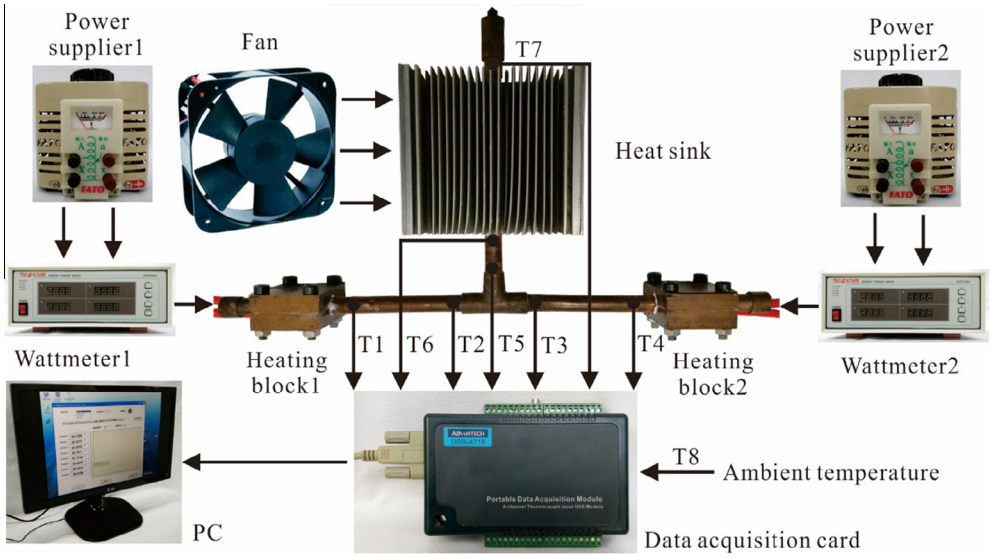

Fig. 3. Heat pipe test apparatus and arrangement.

where k, A and ΔH is the thermal conductivity, the wrapped area and the thickness of the adiabatic cotton, ΔT_i is the temperature difference across the adiabatic cotton layer, i is the serial number of continuous measurement time interval $\Delta\tau$, n is the totality of the time intervals during testing process.

Considering each uncertainty and using square formula to obtain the temperature measurement uncertainty [30]:

$$U_T = \sqrt{\left(\frac{dT}{T_{ave}}\right)^2 + \left(\frac{dW_{power}}{Q}\right)^2 + \left(\frac{dT_{date}}{T_{ave}}\right)^2 + \left(\frac{dQ_{ac}}{Q}\right)^2} \tag{13}$$

where T_{ave} is the time-averaged temperature of each temperature measurement point.

3. Results and discussions

3.1. Effects of working fluid filling ratios to the MBHP

Working fluid filling ratio is an important factor on heat transfer performance of heat pipe and the filling ratio $\eta = 100\%$ is defined as the working fluid fills the whole pore volume of the sintered copper powder in this paper. Six different filling ratio, 50%, 75%, 100%, 125%, 150% and 175%, are tested in this experiment, as show in Fig. 4. We use x $W(L)$ and y $W(R)$ to denote that the input power of heat source 1 and heat source 2 is x W and y W, respectively. In this test, the total heating load is $Q = xW(L) + yW(R)$. Additionally, heat flux q of MBHP can be calculated as below.

$$q = \frac{4Q}{\pi D^2} \tag{14}$$

where D is the outer diameter of the copper tube.

There are many differences among the six filling ratios as show in Fig. 4. The temperature differences between evaporator and condenser increase significantly with the variation of heating load. For instance, the temperature differences of filling ratio 50%, 75%, 100%, 125%, 150% and 175% are from (a) 6.1 °C, (b) 3.3 °C, (c) 7.2 °C, (d) 12.2 °C, (e) 26.1 °C and (f) 54.1 °C at the heating load of 30 W to (a) 7.9 °C, (b) 6.8 °C, (c) 9.2 °C, (d) 28.9 °C, (e) 37.1 °C and (f) 87.9 °C at the heating load of 70 W. It can be seen that MBHP of the filling ratio 75% has best isothermal performance at the same heating load among all the tested filling ratios.

When the filling ratio is 50%, as show in Fig. 4(a), the maximum heating load can reach 100 W and the peak temperature is about 76 °C at the outlet of two evaporators. The maximum heat flux is about 198.9 W/cm^2. When the heating load is higher than 100 W, the evaporator will dry out and the peak temperature will raise quickly. When the filling ratio is 75%, as show in Fig. 4(b), the maximum heating load can reach 160 W and the peak temperature is about 110 °C. The maximum heat flux is about 318.3 W/cm^2. In the Fig. 4(c), the filling ratio is 100%, the maximum heating load, the peak temperature and the maximum heat flux are 160 W, 113 °C and 318.3 W/cm^2, respectively. In the Fig. 4(d), the filling ratio is 125%, the maximum heating load, the peak temperature and the maximum heat flux refer to 100 W, 103 °C and 198.9 W/cm^2, respectively. In the Fig. 4(e), the filling ratio is 150%, the maximum heating load, the peak temperature and the maximum heat flux are 100 W, 103 °C and 198.9 W/cm^2, respectively. In the Fig. 4(f), the filling ratio is 175%, the maximum heating load, the peak temperature and the maximum heat flux refer to 70 W, 113 °C and 139.2 W/cm^2, respectively. To sum up, as the filling ratio increases from 25% to 175%, the maximum heating load also increases at the beginning and then gradually decreases. And the optimal filling ratio is between 75% and 100% which can reach the maximum heating load of 160 W. The following is a description of the reasons for the above phenomena: As the filling ratio of heat pipe is less and the heating load is increasing constantly, condensed liquid flows back to the evaporator and the liquid is boiling vigorously, consequently, the working fluid which does not reach the evaporator section has been evaporated. Evaporated working fluid is more than the backflow in the evaporator section. And then the evaporator appears dry out, tube temperature will rise rapidly and the heat transfer efficiency decreased. Conversely, high filling ratio and constant heat flux will cause a large number of liquid converted to vapor. The pressure inside vapor line becomes large with the density of vapor increasing and it hinders reflux velocity of the condensed liquid. Finally, the continuous cycle rate of the working fluid is affected, so that the temperature at the outlet of evaporator rises rapidly and it also reduces the heat transfer efficiency. Above all, too much or too little of the fill rates are not conducive to effective heat transfer and the optimal filling ratio is between 75% and 100% in this paper.

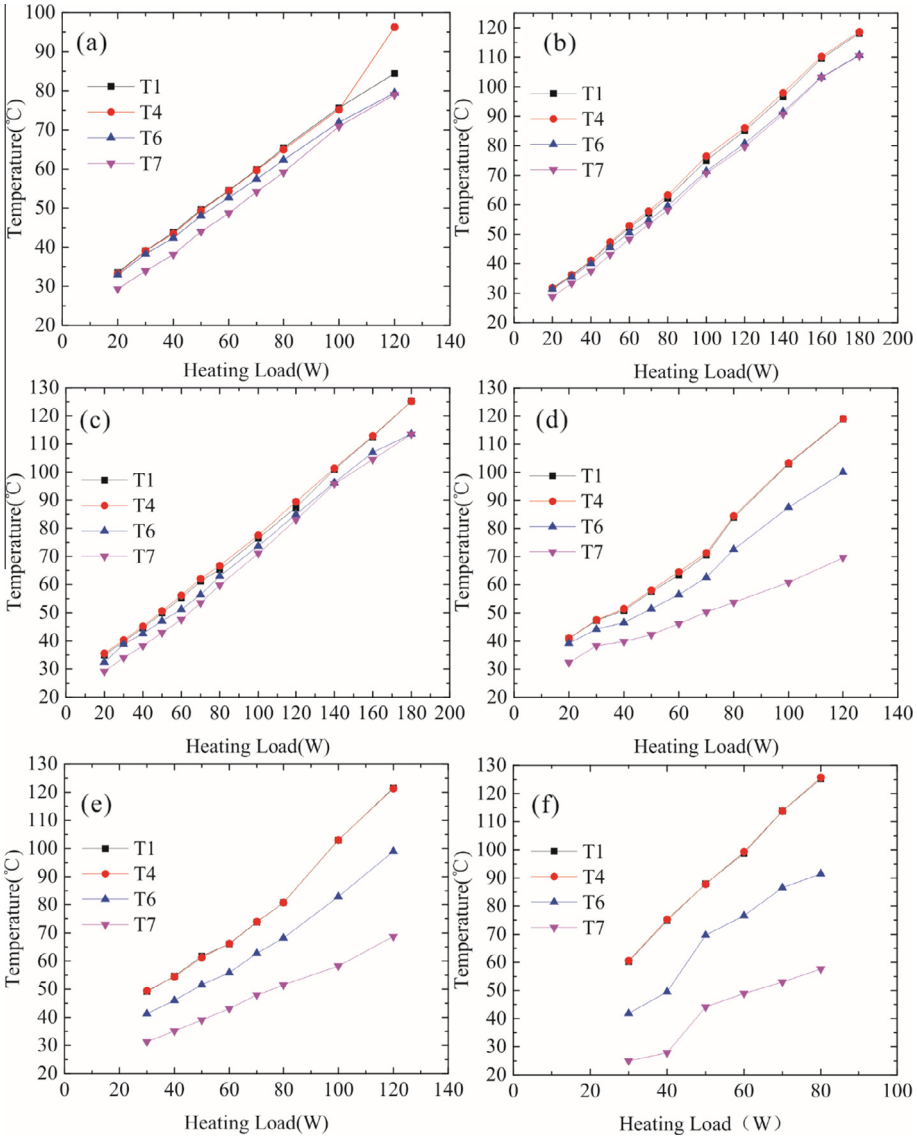

Fig. 4. Thermal performance of MBHP with different working fluid filling ratios: (a) filling ratio 25%, (b) filling ratio 75%, (c) filling ratio 100%, (d) filling ratio 125%, (e) filling ratio 150%, (f) filling ratio 175%.

3.2. Start-up characteristics of the MBHP

The start-up characteristics of the heat pipe are associated with two critical parameters: Start-up time and start-up temperature-rise. Start-up time is the period from the moment the evaporators start to get heated to the moment when their temperatures are stable. Start-up temperature-rise is the temperature difference of the evaporators before and after the startup. In Fig. 5, the filling ratio of MBHP is 75% and the time after the evaporators are heated up can be divided into two parts: the start-up stage and the stable stage. It can be seen that there is no temperature oscillation or overshoot in the MBHP during the start-up stage. Moreover, the start-up time of MBHP is all within 10 min at the total heating load from 30 W to 160 W. The start-up temperature-rise of the heat pipe are (a) 10.8 °C, (b) 27.2 °C, (c) 50.5 °C, (d) 84.6 °C at the heating load (a) 30 W, (b) 60 W, (c) 100 W, (d) 160 W, respectively, in Fig. 5.

In Fig. 6, the filling ratio of MBHP is 175% and the volume of working fluid is larger than the copper pore volume in this case. In Fig. 6, the start-up time and start-up temperature-rise of the heat pipe are (a) 23 min and 44 °C, (b) 20 min and 51 °C, (c) 16 min and 74 °C, (d) 15 min and 87 °C at the heating load (a) 30 W, (b)40 W, (c)60 W, (d)70 W, respectively. It can be seen that as the total power of the heat sources increases, the heat pipe start-up time decreases and the start-up speed increases. This can be explained by the fact that the increase in the heat source power accelerates the speed of the working fluid in evaporators vaporizing into gas. As the vapor volume accumulates, the pressure in the vapor lines rises, accelerating vapor condensation in the condenser. The condensed liquid then returns to the evaporators because of the relatively high capillary pressure between the wetting pores of the condenser and the drying pores of the evaporators. Therefore, with the increase in both the vaporizing and returning speeds of the working fluid, the start-up time of the heat pipe is shortened and the start-up characteristics are improved. It is clear from the start-up characteristics of the MBHP that, for each of the multiple heat sources, in order to reach a stable working state in a shorter time, increasing the power within the allowable limit is the primary choice to be considered. As Fig. 6 shows, the time after the heat pipe evaporators are heated up can be divided into two parts, i.e., the start-up stage and the stable stage (stage 3), where the start-up stage further includes the temperature jump

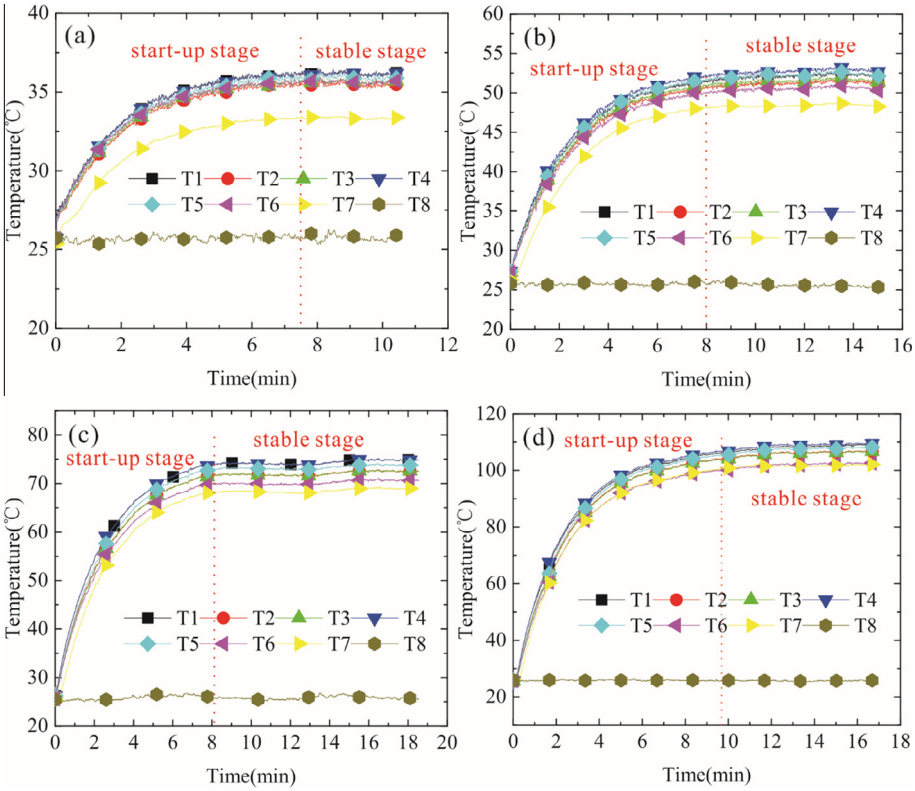

Fig. 5. MBHP (filling ratio 75%) startup under various heat loads (a) 15 *W*(*L*) and 15 *W*(*R*), (b) 30 *W*(*L*) and 30 *W*(*R*), (c) 50 *W*(*L*) and 50 *W*(*R*), (d) 80 *W*(*L*) and 80 *W*(*R*).

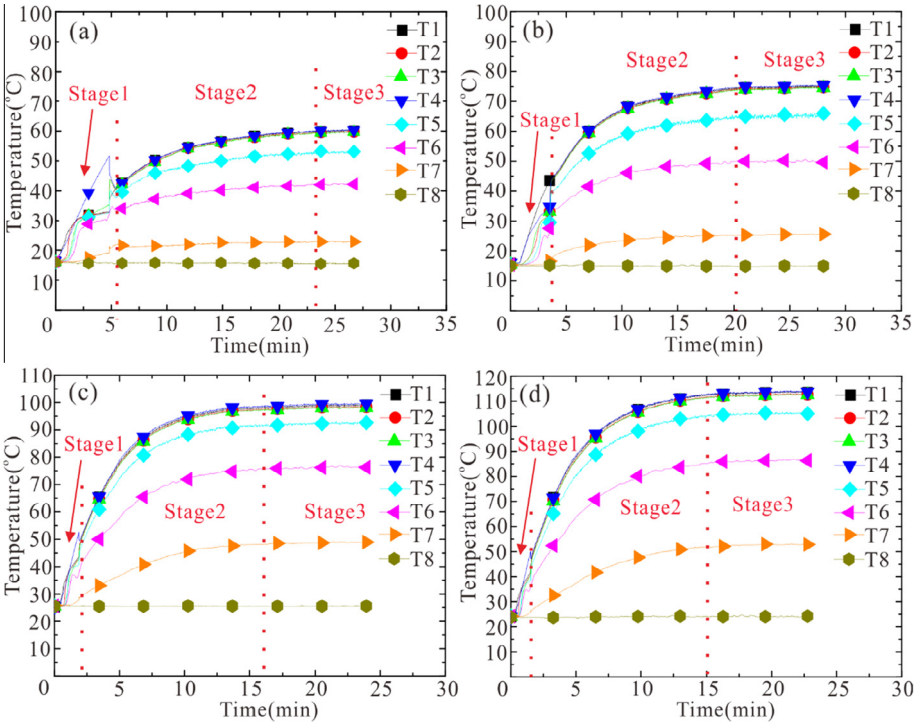

Fig. 6. MBHP (filling ratio 175%) startup under various heat loads (a) 15 *W*(*L*) and 15 *W*(*R*), (b) 20 *W*(*L*) and 20 *W*(*R*), (c) 30 *W*(*L*) and 30 *W*(*R*), (d) 35 *W*(*L*) and 35 *W*(*R*).

stage (stage 1) and the temperature climb stage (stage 2). Both duration and performance degree of the temperature jump stage (stage 1) are related to the heat source power, where duration can be defined as the period during which the temperatures of the two evaporators evolve from different values to become the same and performance degree can be defined as the ratio of the maximum temperature of stage 1 to the stable temperature of satge3. In Fig. 6(a), when the total power of the heat sources is 30 W, the duration of stage 1 is approximately 330 s, the highest temperature of evaporators during stage1 is 51 °C, the steady-state

temperature is 61 °C, and the performance degree of stage 1 is 83.6%. In Fig. 6(b), when the total power of the heat sources is 40 W, the duration of stage 1, the highest temperature of jump, the steady-state temperature and their performance degree are 220 s, 43 °C, 75 °C and 57.3%, respectively. In Fig. 6(c), under the total power of 60 W, the duration of stage 1 is 130 s, the highest temperature of the jump is 52 °C, the steady-state temperature is 99 °C, and the performance degree is 52.5%. As Fig. 6(d) shows, when the total power is 70 W, the duration, highest temperature of jump, steady-state temperature and their performance degree are 100 s, 50 °C, 113 °C and 44.2%, respectively. It can be observed from the data above that there is obvious temperature jump in low-power regions. With the increase in power, the duration and performance degree of stage 1 both decrease. When the total power is greater than 40 W, the effect of temperature jump can be ignored. The reason for the temperature jump stage is explained below. Before the evaporators of the heat pipe are heated, the volume of working fluid is larger than the copper pore volume at the filling ratio 175% and the extra working fluid is left in the steam line. Owing to the effects of those incontrollable factors such as the random distribution of sintered copper powder pores, manufacturing error and gravity, maintaining the distribution proportions of the phase-exchange working fluid in the two evaporating sections the same is difficult. When the heat pipe begins to be heated, the powers of the heat sources loaded on both sides are the same; that is, the vapor volumes of the working fluid in both evaporators are equal at the beginning of heating. Assuming that the volumes of working fluid returning from the condenser to each evaporator are also the same, then it can be ascertained that the temperature of the evaporator with more working fluid climbs more slowly because the extra working fluid absorbs energy to vaporize, shown as the T1 curve in Fig. 6(a). On the other hand, the temperature of the other evaporator increases faster as it contains less working fluid to vaporize, illustrated by the T4 curve of Fig. 6(a). When the extra working fluid in the evaporator with the lower temperature completely vaporizes (T4 reaches the peak of the temperature jump), the vaporizing and returning volumes of both evaporators are the same, respectively. Thereby, the T4 temperature curve begins to fall significantly while the T1 curve begins to increase more rapidly. Finally, both evaporators reach steady state with the same temperature-rise speed. The description above illustrates that this type of heat pipe may exhibit slight fluctuations at the start-up stage under low-power conditions at the high filling ratio.

To sum up, the MBHP proposed and manufactured in this work meets the requirement of multi-heat source heat dissipation of electronic devices. It is able to guarantee the highest temperature at under 110 °C when the total power of the heat sources is below 160 W with the optimal filling ratio. For many electronics, for example LED with the maximum junction temperature of 150 °C [31], this temperature is a reliable condition to ensure normal lifetime of products.

3.3. Power distribution characteristics of the MBHP

In Fig. 7, the filling ratio of MBHP is 75%. The power of heat source 1 and heat source 2 for the heat pipe is (a) 10 $W(L)$ and 110 $W(R)$, (b) 30 $W(L)$ and 90 $W(R)$, (c) 50 $W(L)$ and 70 $W(R)$, and (d) 60 $W(L)$ and 60 $W(R)$, respectively. The total power of the two heat sources in each group above is 120 W.

When the sum of the power of the two heat sources is 120 W, regardless of how the power of the two heat sources is allocated, the steady-state temperature of the heat pipe is always the same. The peak temperature and the start-up temperature-rise of MBHP are 86 °C and 60.9 °C. When the power of the two heat sources for the MBHP have the same sum but different distributions, the heat pipe has the same steady-state temperature in the range of allowable error. This is because an increase in the total energy in a system must be equal to the difference between the energy entering and exiting the system. If the energy entering a system is equal to the energy leaving the system, then the energy increase of the system is zero and the same final system state will be reached. Therefore, in the case with the same total power and the same condensing conditions, the steady-state temperature eventually reaches must be equal.

Therefore, it can be concluded that the MBHP proposed in this paper is capable of satisfying the demand of electronics working in the same environment with various power values, as well as ensuring the same lifetime under different working conditions. The overall performance of electronics can thereby be effectively improved.

3.4. Dynamic response characteristics of the MBHP

In this experiment, the filling ratio of MBHP is 75% and the heating load of the two heat sources is continuously changed to observe the temperature variation trend, as shown in Fig. 8. It can be seen that the heating loads of the two heat sources are S1: 30 $W(L)$ & 0 $W(R)$, S2: 30 $W(L)$ & 30 $W(R)$, S3: 60 $W(L)$ & 30 $W(R)$, S4: 60 $W(L)$ & 60 $W(R)$, S5: 30 $W(L)$ & 60 $W(R)$, S6: 30 $W(L)$ & 30 $W(R)$, S7: 0 $W(L)$ & 30 $W(R)$, S8: 0 $W(L)$ & 0 $W(R)$, where S1: 30 $W(L)$ & 0 $W(R)$ represents the state (S1) with the power of heat source1 being 30 W and heat source 2 being 0 W.

As can be seen that S1 in the Fig. 8, the input power of heat source 1 increased from 0 to 30 W while the input power of heat source 2 is still 0 W, resulting all the curves rising steadily at the same time. The peak temperature reaches a steady temperature of 42.1 °C with temperature difference ΔT = 16.8 °C. However, the temperature rise of the T4 curve is not as significant as that of the T1 curve. This is because S1 is the stage that the heat pipe is heated by the two heat sources with a power of 30 $W(L)$ and 0 $W(R)$, respectively, as Fig. 8 shows. Both heat source 2 and the condenser are heat sinks relative to heat source 1. The heat transfer direction suggests that a small amount of heat is transferred from heat source 1 to heat source 2. At this moment, the branch corresponding to heat source 2 is equivalent to being heated by heat source 1. Consequently, the T4 curve of S1 in Fig. 8 exhibits a slowly increasing trend. Compared with heat sources 1 and 2, the heat sink on the third branch always has a relatively low temperature. Therefore, most of the energy in heat source 1 is transferred to the condenser. Although a small amount of energy is transferred from heat source 2 to the condenser, it primarily serves as a heating object in the start-up stage. However, the heat sink continuously transfers heat out through the heat exchange with the surrounding environment. The majority of the energy generated by heat source 1 is transferred to the heat sink while only a small part is used to heat the branch of heat source 2. Therefore, the overall start-up speed of the T4 curve is relatively low.

When the power of heat source 2 is also increased from 0 W to 30 W, the temperature curve steadily increases from state S1 to state S2. The peak temperature of MBHP varies from the original steady temperature of 42.1 °C to a new steady temperature of 55.6 °C with a temperature difference ΔT = 13.5 °C. When the power of heat source 1 is increased from 30 W to 60 W, the temperature curve steadily increases from state S2 to state S3 and the peak temperature reaches a new steady temperature of 70.3 °C with temperature difference ΔT = 14.7 °C. When the power of heat source 2 is also increased from 30 W to 60 W, the temperature curve steadily increases from state S3 to state S4 and the peak temperature reaches a new steady temperature of 86.6 °C with temperature difference ΔT = 16.3 °C. At this point, the power values of the heat sources are both 60 W and the corresponding temperatures are in the steady state. The power of heat source 1

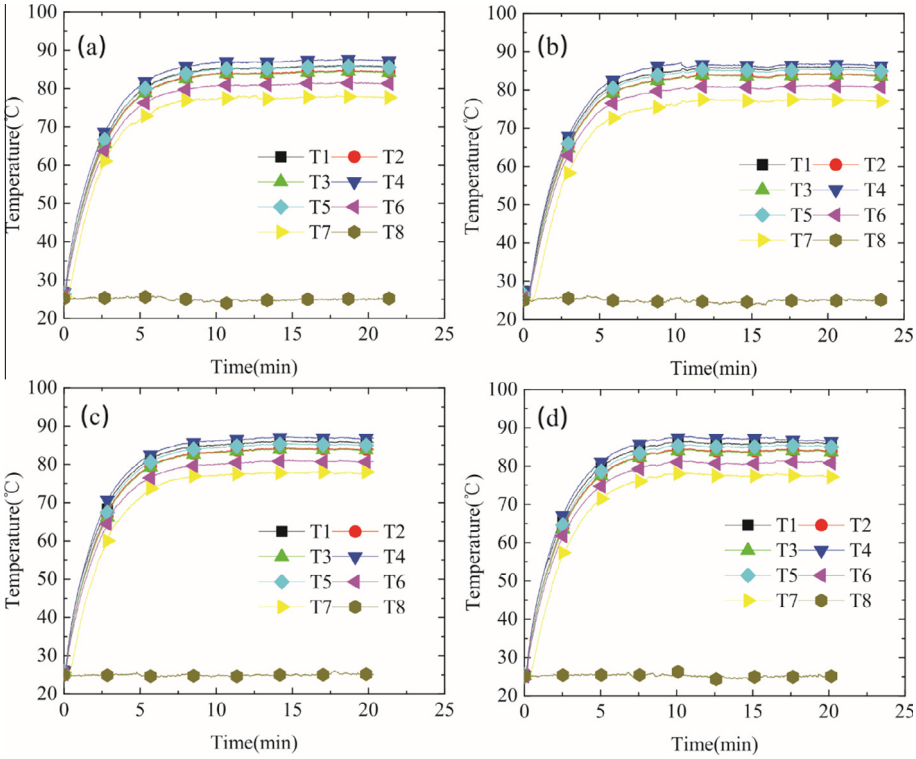

Fig. 7. MBHP (filling ratio 75%) startup under a constant total power: (a) 10 *W*(*L*) and 110 *W*(*R*), (b) 30 *W*(*L*) and 90 *W*(*R*), (c) 50 *W*(*L*) and 70 *W*(*R*), (d) 60 *W*(*L*) and 60 *W*(*R*).

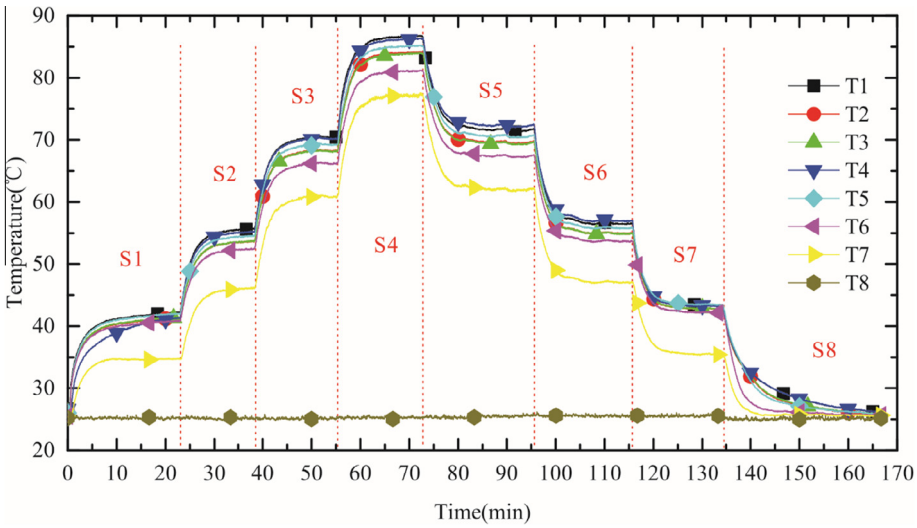

Fig. 8. Dynamic characteristics of the MBHP (filling ratio 75%) with heating load increasing from 0 W to 120 W before decreasing from 120 W to 0 W.

subsequently rapidly decreases from 60 W to 30 W, with the temperature curve changing from state S4 to state S5, as shown in Fig. 8. A new steady temperature of state S5 is the same as the peak temperature of state S3. When the heat pipe temperature is steady, the power of heat source 2 decreases from 60 W to 30 W, driving the curve from state S5 to state S6, and so on. Thus, it is clear that in a working heat pipe, when the heating power of a branch is changed, the temperature of each branch could steadily increase or decrease to a new steady temperature over time.

The dynamic characteristics of the MBHP (filling ratio 75%) with the total heating load increasing from 20 W to 180 W, progressively, are shown in Fig. 9. It is clear from the above test and analysis that the dynamic response characteristics of the MBHP can be applied in the field of heat dissipation of power-varying multi-heat source systems. The power of multiple heat sources can be adjusted in accordance with the requirements of the practical situation. Regardless of how the requirement varies, the working conditions of multiple heat sources can be kept consistent through MBHPs. The MBHP proposed in this research can ensure that multi-heat source electronics operate as designed in environments with frequent power variations. When the power of the heat sources increases, the heat pipe can force each branch to transfer to new steady states. When the power decreases, the heat pipe can also provide some buffer and protection.

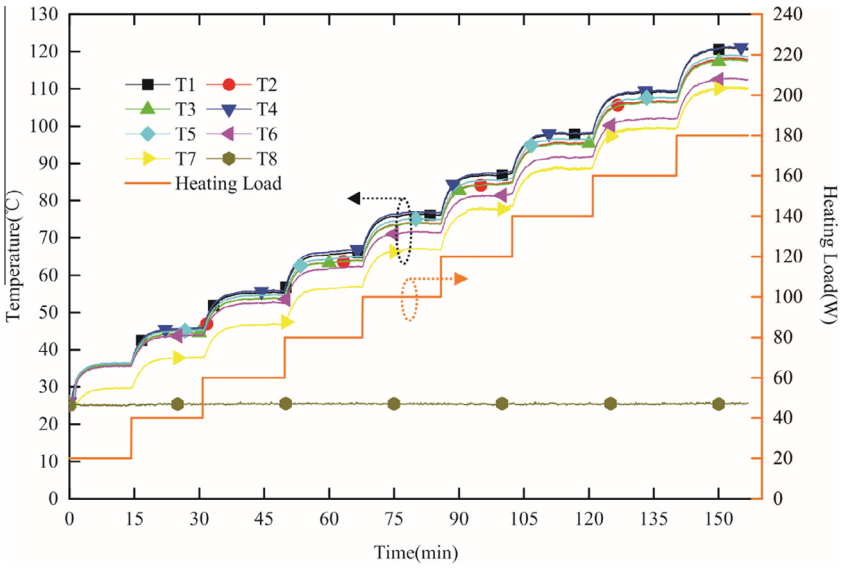

Fig. 9. Dynamic characteristics of the MBHP (filling ratio 75%) with heating load increasing from 20 W to 180 W.

3.5. Thermal resistance analysis of the MBHP

Thermal resistance is a crucial technical index describing the heat transfer characteristics of electronics, which refers to the ratio of the temperature difference between two points to the power that generates this temperature difference under the thermal balance [32]:

$$R = \frac{\Delta T}{Q} \tag{15}$$

Fig. 10(a) is a schematic of the thermal resistance distribution of the proposed MBHP. The calculations are based on the following equations:

$$R_1 = \frac{2(T_1 - T_5)}{Q} \tag{16}$$

$$R_2 = \frac{2(T_4 - T_5)}{Q} \tag{17}$$

$$R_3 = \frac{(T_5 - (T_6 + T_7)/2)}{Q} \tag{18}$$

$$R_{tot} = \frac{\Delta T}{Q} = \frac{R_1 R_2}{R_1 + R_2} + R_3 = \frac{(T_1 + T_4)/2 - (T_6 + T_7)/2}{Q} \tag{19}$$

where R_1 and R_2 are the thermal resistance from heat source 1 and heat source 2 to the concourse of two branches, respectively; R_3 is the thermal resistance from the concourse to the condenser; R_{tot} is the total thermal resistance of the heat pipe; R_1 and R_2 are connected in parallel prior to being connected with R_3 in series; Q is the total heating load and ΔT is the total temperature difference of the heat pipe.

As shown in Fig. 10(b), they are the thermal resistances of six filling ratios at each heating load. the total thermal resistances of filling ratio 50%, 75%, 100%, 125%,150% and 175% are from 0.1 °C/W, 0.06 °C/W, 0.12 °C/W, 0.2 °C/W, 0.92 °C/W and 54.1 °C/W at the heating load of 30 W to 0.06 °C/W, 0.05 °C/W, 0.1 °C/W, 0.2 °C/W, 0.27 °C/W and 0.63 °C/W at the heating load of 70 W. Moreover, it can be observed from Fig. 10(b) that the optimal filling ratio is between 75% and 100%. In this range of filling ratios, thermal resistance can achieve the minimum and limit of heating load could reach the maximum. With the increase in the total power, the thermal resistance of the heat pipe gradually declines and reaches a minimal value. For instance, when the filling ratio of MBHP is 75%, the total thermal resistance can reach $R_{tot} = 0.08$ °C/W under a heating load of 20 W at the beginning and then gradually declines to the minimum $R_{tot} = 0.04$ °C/W at the heating load of 160 W. This is because the constantly increasing heating power of the heat pipe accelerates vaporization of the working fluid in evaporators, leading to a continuous increase

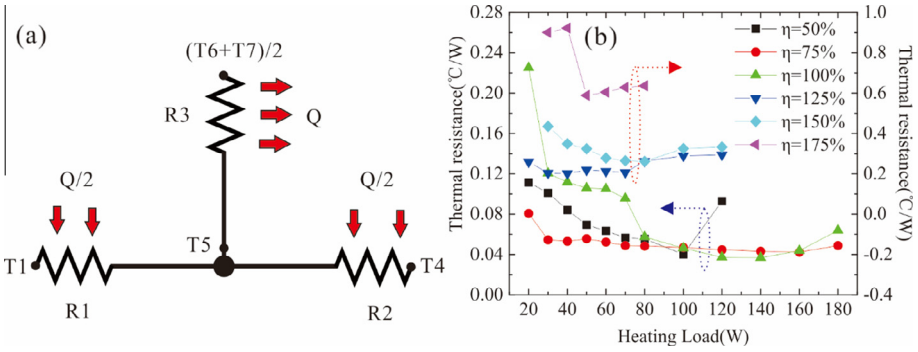

Fig. 10. (a) Thermal resistance distribution and (b) thermal resistances of six filling ratios corresponding to the thermal load of the MBHP.

in vapor pressure in the vapor lines. The pressure increase then forces the vapor to condense more rapidly in the condenser. The pressure difference between the capillary wicks of the condenser and the evaporators also constantly increases, which causes the working fluid to flow back into the capillary wicks rapidly and gradually reduce the total thermal resistance. However, with the further increase in the total power, only a slight increase occurs in the thermal resistance of the heat pipe. For example, when the filling ratio of MBHP is 75%, the total thermal resistance under total power value of 180 W is about 0.05 °C/W, respectively, which has a slight increase compared with the minimal value 0.04 °C/W. This is mainly because with the further power increase, the local dry-out phenomenon occurs in the evaporators, causing a slight increase in the thermal resistance [29]. As a result, the heat transfer performance of the heat pipe will degrade.

4. Conclusions

This paper presented the results of tests conducted on a newly developed MBHP consisting of two evaporators and a condenser, which is primarily suited for heat dissipation in multi-heat source electronics. The following conclusions were drawn from the results obtained:

(1) The filling ratio has a great influence on the heat transfer performance of heat pipe and the optimal filling ratio is between 75% and 100% in this paper. Under this range of filling ratios, the MBHP can start up rapidly and reach the stable heat transfer for the multi-heat sources.
(2) The optimum working heating load of the proposed MBHP is in the range 30–160 W. In particular, for a total heating load from two heat sources of 160 W, the heat pipe can reach its optimum heat transfer performance with the minimum thermal resistance of 0.04 °C/W, the maximum heat flux of 318.3 W/cm^2 and the highest temperature below 110 °C, which is considered a reliable condition for safe operation of most electronics, such as high-power LED.
(3) When the heat sources on both sides of the heat pipe are equal in terms of total power, regardless of how the power of the two heat sources is allocated, the final steady-state temperature in the heat pipe remains the same.
(4) After the MBHP starting up, regardless of whether the heat source power increases or decreases, the temperature of each branch can steadily rise or fall to a new steady value without any sudden temperature change. Therefore, it can be applied in situations where the multi-heat source power varies frequently and consistent working environment and lifetime are required among heat sources.

Acknowledgments

This work is supported by National Natural Science Foundation of China (No. U1401249 and No. 51375177), Postdoctoral Science Foundation of China (No. 2015T80904), Fundamental Research Funds for the Central Universities, and Natural Science Foundation of Guangdong Province (No. 2014A030312017).

References

[1] S.V. Garimella, A.S. Fleischer, J.Y. Murthy, A. Keshavarzi, Thermal challenges in next-generation electronic systems, Compon. Packag. Technol. IEEE Trans. 31 (4) (2008) 801–815.
[2] D.A. Reay, Heat pipes, Phys. Technol. 16 (2) (1985) 69.
[3] L.L. Vasiliev, Heat pipes in modern heat exchangers, Appl. Therm. Eng. 25 (1) (2005) 1–19.
[4] A. Faghri, Review and advances in heat pipe science and technology, J. Heat Transfer 134 (12) (2012) 723–732.
[5] S.H. Noie, Heat transfer characteristics of a two-phase closed thermosyphon, Appl. Therm. Eng. 25 (4) (2005) 495–506.
[6] D. Wang, Z. Liu, S. He, J. Yang, W. Liu, Operational characteristics of a loop heat pipe with a flat evaporator and two primary biporous wicks, Int. J. Heat Mass Transfer 89 (2015) 33–41.
[7] S.C. Wong, C.W. Chen, Visualization experiments for groove-wicked flat-plate heat pipes with various working fluids and powder-groove evaporator, Int. J. Heat Mass Transfer 66 (6) (2013) 396–403.
[8] K.H. Chien, Y.T. Lin, Y.R. Chen, K.S. Yang, C.C. Wang, A novel design of pulsating heat pipe with fewer turns applicable to all orientations, Int. J. Heat Mass Transfer 55 (s21–22) (2012) 5722–5728.
[9] G. Wang, D. Mishkinis, D. Nikanpour, Capillary heat loop technology: space applications and recent Canadian activities, Appl. Therm. Eng. 28 (4) (2008) 284–303.
[10] S.J. Dong, Y.Z. Li, J. Wang, J. Wang, Fuzzy incremental control algorithm of loop heat pipe cooling system for spacecraft applications, Comput. Math. Appl. 64 (5) (2012) 877–886.
[11] M. Esen, H. Esen, Experimental investigation of a two-phase closed thermosyphon solar water heater, Sol. Energy 79 (5) (2005) 459–468.
[12] T. Brahim, M.H. Dhaou, A. Jemni, Theoretical and experimental investigation of plate screen mesh heat pipe solar collector, Energy Convers. Manage. 87 (2014) 428–438.
[13] M.F. Remeli, L. Tan, A. Date, B. Singh, A. Akbarzadeh, Simultaneous power generation and heat recovery using a heat pipe assisted thermoelectric generator system, Energy Convers. Manage. 91 (91) (2015) 110–119.
[14] V.G. Pastukhov, Y.F. Maidanik, C.V. Vershinin, M.A. Korukov, Miniature loop heat pipes for electronics cooling, Appl. Therm. Eng. 23 (9) (2003) 1125–1135.
[15] J.-C. Wang, U- and L-shaped heat pipes heat sinks for cooling electronic components employed a least square smoothing method, Microelectron. Reliab. 54 (6–7) (2014) 1344–1354.
[16] X.Y. Lu, T.C. Hua, M.J. Liu, Y.X. Cheng, Thermal analysis of loop heat pipe used for high-power LED, Thermochim. Acta 493 (s 1-2) (2009) 25–29.
[17] J. Shen, J. Fang, H. Sips, A.L. Varbanescu, An application-centric evaluation of OpenCL on multi-core CPUs, Parallel Comput. 39 (12) (2013) 834–850.
[18] Y.F. Fung, M.F. Ercan, T.K. Ho, W.L. Cheung, Performance optimization for parallel processing on a multiple-CPU server, Comput. Phys. Commun. 142 (1–3) (2001) 191–195.
[19] R.J. McGlen, R. Jachuck, S. Lin, Integrated thermal management techniques for high power electronic devices, Appl. Therm. Eng. 24 (8–9) (2004) 1143–1156.
[20] Y. Wang, K. Vafai, An experimental investigation of the thermal performance of an asymmetrical flat plate heat pipe, Int. J. Heat Mass Transfer 43 (19) (2000). 3753-3753.
[21] B.K. Tan, T.N. Wong, K.T. Ooi, Analytical effective length study of a flat plate heat pipe using point source approach, Appl. Therm. Eng. 25 (14–15) (2005) 2272–2284.
[22] W.B. Bienert, D.A. Wolf, M.N. Nikitkin, Y.F. Maidanik, Y. Fershtater, S. Vershinin, J.M. Gottschlich, The proof-of-feasibility of multiple evaporator loop heat pipes, in: Proceedings of the Sixth European Symposium on Space Environmental Control Systems, 400, 1997, pp. 393–398.
[23] D. Bugby, K. Wrenn, D. Wolf, E. Kroliczek, J. Yun, S. Krein, D. Mark, Multi-evaporator hybrid loop heat pipe for small spacecraft thermal management, in: Aerospace Conference, 2005, pp. 810–823.
[24] S. Okutani, H. Nagano, S. Okazaki, H. Ogawa, H. Nagai, Operating characteristics of multiple evaporators and multiple condensers loop heat pipe with polytetrafluoroethylene wicks, J. Electron. Cooling Therm. Control 4 (2014) 22–32.
[25] E. Habtour, M. Nikitkin, Miniature multiple evaporator multiple condenser loop heat pipe, in: AIAA Conference on Small Satellites, 2005.
[26] Y. Tang, R. Zhou, L. Lu, Z. Xie, Anti-gravity loop-shaped heat pipe with graded pore-size wick, Appl. Therm. Eng. 36 (2012) 78–86.
[27] Y. Li, S. Chen, B. He, Y. Yan, B. Li, Effects of vacuuming process parameters on the thermal performance of composite heat pipes, Appl. Therm. Eng. 99 (2016) 32–41.
[28] Y. Li, Z. Li, C. Chen, Y. Yan, Z. Zeng, B. Li, Thermal responses of heat pipes with different wick structures under variable centrifugal accelerations, Appl. Therm. Eng. 96 (2016) 352–363.
[29] H. Li, B. Zhou, Y. Tang, R. Zhou, Z. Liu, Y. Xie, Effect of working fluid on heat transfer performance of the anti-gravity loop-shaped heat pipe, Appl. Therm. Eng. 88 (2015) 391–397.
[30] S.J. Kline, The purposes of uncertainty analysis, J. Fluids Eng. 107 (2) (1985) 153–160.
[31] D. Gacio, J.M. Alonso, J. Garcia, M.S. Perdigao, E.S. Saraiva, F.E. Bisogno, Effects of the junction temperature on the dynamic resistance of white LEDs, Ind. Appl. IEEE Trans. 49 (2) (2013) 750–760.
[32] L. Jiang, J. Ling, L. Jiang, Y. Tang, Y. Li, W. Zhou, J. Gao, Thermal performance of a novel porous crack composite wick heat pipe, Energy Convers. Manage. 81 (2) (2014) 10–18.